

## JOINING BEHAVIOUR OF THICK PLATE USING HIGH-FREQUENCY INDUCTION ASSISTED ARC WELDING

Combining a preheating source with conventional arc welding is a promising method to study the weld quality and improvement of strength for high-strength super-alloy materials. The present research used an induction preheating source with plasma arc welding (PAW) to weld Inconel 625 thick plates. The investigation was performed at a constant induction current of 600 A, welding speed of 100 mm/min and a plasma welding current of 135 A. The induction-assisted plasma arc welding (IAPAW) demonstrated that a weld joint was possible with static induction preheating and a high plasma welding current at low welding speed. The microstructural observation showed various dendritic structures in the fusion zone (FZ). The FESEM and EDX analysis confirmed the formation of Laves phase in the interdendritic structure of the FZ. The ultimate tensile strength of the IAPAW joint reached to 658 MPa. The tensile fracture surface of the welded sample revealed a lower number of dimples, indicating the reduction of ductility. The XRD analysis was carried out at various zones and it confirmed the peak shifting towards the higher 2-theta value of the FZ.

*Keywords:* Induction heating; plasma arc welding; hybrid welding; microstructure; tensile test

### 1. Introduction

#### 1.1. Inconel 625 welding

Inconel 625 superalloy is a Ni-base solid solution hardenable material. They are primarily strengthened by adding substitutional elements like Cr, Mo, and Fe in the austenitic matrix. Many researchers have reported that this material has high strength and toughness from cryogenic temperatures to elevated temperatures, *i.e.*, up to 1100°C. This alloy has high tensile, fatigue, thermal fatigue, creep and rupture strength. In addition to mechanical properties, this alloy offers outstanding corrosion resistance at elevated temperatures. These characteristics make the Inconel 625 ideal for various industries, including geothermal, marine, power generation, aerospace, chemical processing, nuclear etc. [1]. The alloying elements Nb, Mo, and Ti improve mechanical characteristics at low and high temperatures. Additionally, alloy 625 has improved weldability and fabricability. As a result, this material is highly desirable for industrial applications [2]. In FZ, the variations of alloying elements like Nb, Mo, Ti Ta, Fe and C in the austenitic matrix strongly influence the number of secondary phases ( $\gamma$  + metal carbides (MCs) + Laves) formation during the solidification. This secondary phase formation reduces the material properties of the welding component [3].

Some of the traditional approaches used to weld nickel-based superalloys are electron beam welding (EBW) [2], laser beam welding (LBW) [4], tungsten inert gas welding (TIG) [5], and recently friction stir welding (FSW) [6]. The effectiveness of joint strength typically depends on the welding process, plate thickness of base material (BM) and the composition of filler material if used [7-8]. The conventional welding method is more adaptable and readily available for welding of nickel-based alloys with a limited thickness. Mostly multi-pass welding is used for highly thick plate, leading to increase of residual stress in the welded sample. In some processes, a suitable filler rod is required to weld thick plates. It results in a significant change of microstructure in the FZ and its properties [9]. These processes produce an enormous amount of heat and compositional variation, which reduce corrosion resistance and weaken mechanical strength and chemical characteristics. Multiple studies have been carried out to evaluate the joint feasibility of Inconel 625 alloy. Han et al. [10] investigated for enhancement of corrosion resistivity with Nb content in the FZ of Inconel 625 welded by shielded metal arc welding. They found no significant improvement in corrosion resistance except for a negligible increase in hardness values as the Nb content rises. Many researchers have found high welding heat input results in segregation of elements in the interdendritic arms [2], liquation cracking or micro-fissuring at the

<sup>1</sup> IIT GUWAHATI, GUWAHATI-781039, INDIA

\* Corresponding email: [dipankar.saha@iitg.ac.in](mailto:dipankar.saha@iitg.ac.in)



heat-affected zone (HAZ) [11], and residual stresses [12]. Hence, the industries have recommended post-weld heat treatment to overcome the aforementioned problem with the high energy density processes, namely EBW [2] and LBW. The current study provides a novel approach for joining Inconel-625 alloy by using induction-assisted plasma arc welding technique.

## 1.2. High-frequency induction assisted welding

Many researchers have studied the performance improvement of manufacturing techniques using preheat, heat-assisted, or post heat methods. A high-frequency induction heating arrangement is the most recommended technique for many types of complex applications with a wide range of materials [13-15]. The high-frequency induction welding (HFIW) process uses high-frequency induction heating principle to join conducting materials with applied load. Frequency plays an essential role in controlling the penetration depth of the FZ. The absence of hazardous fume and gases during welding makes the HFIW process the cleanest welding compared to the conventional and non-conventional arc welding processes. The electrical energy is transferred to the workpiece without direct contact through the induction coil and generate heat directly into the workpiece material. When enough joining temperature is generated in the workpiece material and with the applied load during holding time, a significant joint can achieve [16-17].

The induction heating mechanism works directly with conductive materials. It is easier and faster to weld a ferromagnetic material because of eddy current heating and hysteresis heating. The joining of non-conducting material can also be achieved by using subsector material. The presence of the conducting or magnetic particulate in the polymer material has significantly shown proper and clean joining by this process [18]. In the pipe fabrication process, HFIW is mainly used due to the rapid heating of the faying surfaces, and only workpiece material will heat up during welding. Generally, induction heating is primarily used for heat treatment, furnace sintering, forging, hardening, welding, and heating applications like induction cooking.

A high-frequency alternating current passes through an induction coil, creating an alternating magnetic field in the workpiece material. The alternating magnetic field frequency is similar to the frequency of the current flow through the coil. When alternating magnetic field passes through a conducting material, eddy current is induced, which flows with the same alternating magnetic field frequency through the conducting material. Eddy current ( $I_c$ ) leads to heating in the workpiece, which is  $I_c^2 R$  heating. In addition to the eddy current heating, the ferromagnetic material provides another heating behaviour called hysteresis loss. This behaviour offers heating up to curie temperature; afterwards, the material loses its magnetic properties, and eddy current heating will further carry the heating process. The proximity and edge effects assist in softening the edges of the material.

There is a growing interest in the hybrid welding process due to numerous advantages compared to other conventional

welding processes. Many researchers have integrated the primary welding process with induction heating setups like induction-laser [7,14]; induction-GMAW [13]; induction-friction stir welding [20] etc., to get synergic effect attributes to deeper penetration and controlled microstructure. Ikram et al. [8] investigated the implementation of induction heating process with AC-GMAW process. They found the effectiveness of induction heating as an assistive heat source for AC-GMAW welding of plates thicker than 8 mm. Arif et al. [13] proposed an induction-assisted AC-GMAW process for 6 mm thick plate. They concluded that weld arc irruption and spatter generation were reduced by adopting an external magnetic field generated by a high-frequency induction setup. In addition, controlled heat input through this process provided a solution for welding 5 mm thick plates. Zhang et al. [21] investigated the real-time induction assisted gas tungsten arc underwater welding of 8 mm thick Q460 steel. They found that the external magnetic field has an adverse effect on the weld arc formation and depends on the coil to torch distance. Coelho et al. [14] evaluated the mechanical and metallurgical properties of an induction-assisted laser-welded high strength low alloy (HSLA) steel and two thermo-mechanically treated HSLA plates (i.e., S500MC and S700MC).

The induction-assisted welding process reduces shrinkage and residual stresses that help to minimize cracking and distortion. A weldment that has been properly preheated will be less brittle and more ductile because it is cooled more slowly, as well as less hardness in the HAZ. These qualities are particularly crucial for materials like cast iron, high-carbon steel, or high-carbon equivalent steel that are more prone to hardness at high temperatures. Slowing the cooling rate also allows hydrogen to escape the weld puddle and help to minimize cracking. This provides advantages for thick materials whose heat conduction rate is high.

Nowadays, hybrid welding processes are used to achieve cost-effective joints with superior weld quality. However, there are very few research papers available on the joining of Inconel 625 alloy. There is a need to do research on induction-assisted plasma arc welding of superalloys. This process could be more productive as multi-passes does not require to join highly thick plates. Most of the literature reported autogenous or hybrid welding of limited thickness, up to 5 mm, while laser and electron beam welding reported for higher thickness. However, implementing LBW and EBW techniques for joining thick plates is unsuitable due to the development of residual internal stress and solidification cracking during welding, and the requirement of post-heat treatment.

## 2. Material and methods

This study used a high strength superalloy Inconel 625 with a 6 mm thickness plate to weld with square butt joint configuration by high-frequency induction assisted plasma arc welding setup. The chemical composition (in wt.%) of the BM is listed in TABLE 1.

TABLE 1

Chemical composition (wt.%) of as received Inconel 625 alloy

Ni	Cr	Mo	Nb	Fe	Mn	Al	Ti
57.5	22	9.3	4.6	4.9	1.1	0.3	0.3

The welding experiments were conducted on a indigenously designed, high-frequency induction assisted plasma arc welding setup, as shown in Fig. 1. A high-frequency induction heating machine (make- Ambrell Inc. maximum power 10 kW; model – Easy heat 8310) was used to preheat the faying surfaces in atmospheric conditions. A double-turn rectangular shape ( $20 \times 100 \text{ mm}^2$  dimensions) coil fabricated with copper cylindrical tube (outer diameter and inner diameter are 6 mm and 5 mm) was used. A cooling unit (make – Werner Finley Pvt. Ltd.) was attached to the induction heating machine to draw out the heat generated from the coil. During preheating, a 2 mm coupling gap between the coil and base plate was maintained. Under the effect of the high frequency alternating magnetic field, eddy current heat was generated in the BM plate. Initially, the base plate was static heated for 30 seconds. Afterwards, the base plate was moved to maintain a  $530^\circ\text{C}$  constant temperature with the welding speed below the plasma nozzle. A Fronius plasma arc welding machine (Plasma Module 10 with TransTig 1500) was used with induction-assisted heating. The plasma arc welding system comprises a power source, plasma generator, welding torch and gas supply unit.

For welding, plates were prepared from a Inconel 625 alloy plate using numerically controlled electric discharge machine with rectangular dimensions of  $150 \times 75 \times 6.18 \text{ mm}^3$ . Before welding, the faying surfaces were prepared right-angle to get a square butt configuration. These faying surfaces were ground with emery paper to remove oxide layers and cleaned with acetone to eliminate other impurities. The prepared Inconel plates were placed over a mild steel backing plate and rigidly clamped with four grippers for butt welding. Welding was carried out on a CNC-controlled servo motor-driven bed at a specific welding speed. The welding parameters are listed in TABLE 2. Initially, 30 s static induction heating was applied on the faying surface. After that, the preheated surface was moved towards the weld-

ing touch. In this research, a major investigation was to weld thick Inconel 625 plates in single pass with square butt joint configuration using IAPAW process.

TABLE 2

Parameter for HIPAW Welding

Parameter	Values
Plasma gas flow rate (L/min)	1.0
Plasma current (Amp)	9
Stand-off distance (mm)	4
The gap between the torch and coil (mm)	50
Coupling distance (mm)	2
Induction current (Amp)	600
Static heating time (sec)	30
Welding speed (mm/min)	100
Welding current (Amp)	135
Shielding gas flow rate (L/min)	15

## 2.1. Test and Analysis

After welding, the tensile specimens were extracted from the welded workpiece perpendicular to the weld line using wire electric discharge machining (Make: EC032, JMachine, India) as per the ASTM E8 standard. The tensile test was performed in a BISS 250 KN servo-hydraulic universal testing machine. The fracture surface was examined by field emission scanning electron microscopy (FESEM) (Make: Sigma, Zeiss, Germany). The metallographic samples were prepared according to standard metallographic practices to study the microstructure of the sectioned welded specimens. The specimens were subjected to mechanically polished using abrasive emery papers from rough 220 grit to fine 2500 grit, followed by velvet cloth polishing with  $0.3 \mu\text{m}$  alumina powder to obtain mirror-like polish. Subsequently, polished samples were etched for 30 s with a reagent comprising 15 ml HCl, 10 ml acetic acid, and 10 ml  $\text{HNO}_3$ . The microstructural features of etched welded specimens were examined using optical microscopy (OM). The high magnification images were taken by FESEM. The Energy-dispersive X-ray spectroscopy (EDX) with FESEM was used for point and area

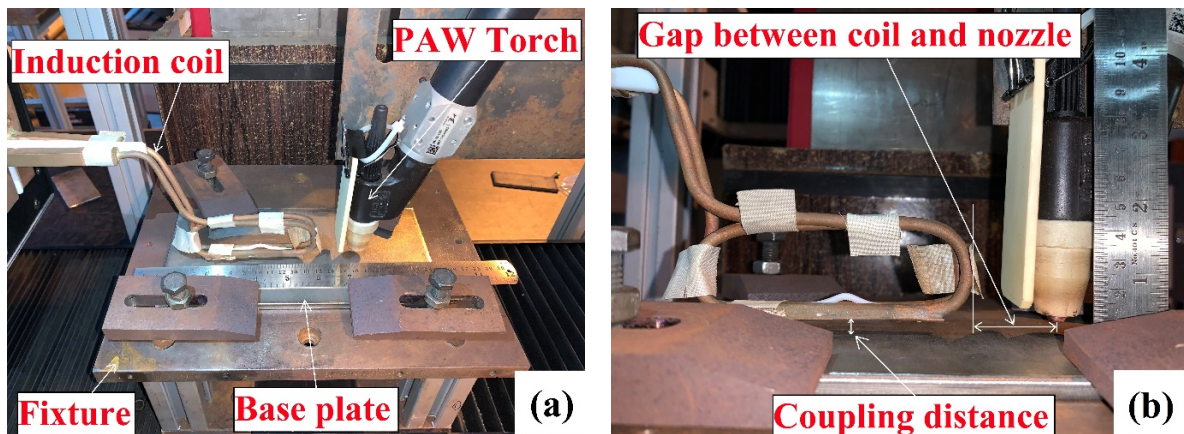


Fig. 1. A high-frequency induction assisted plasma arc welding setup

scan analysis. The diffraction of peaks was analyzed by using X-ray Powder Diffraction (XRD) Cu K radiation at 45 kV and 200 mA. All thin film specimens cut from welded joint were scanned from 20 to 100 degree 2-theta value with a 0.02-degree step size and 3 degree/min speed.

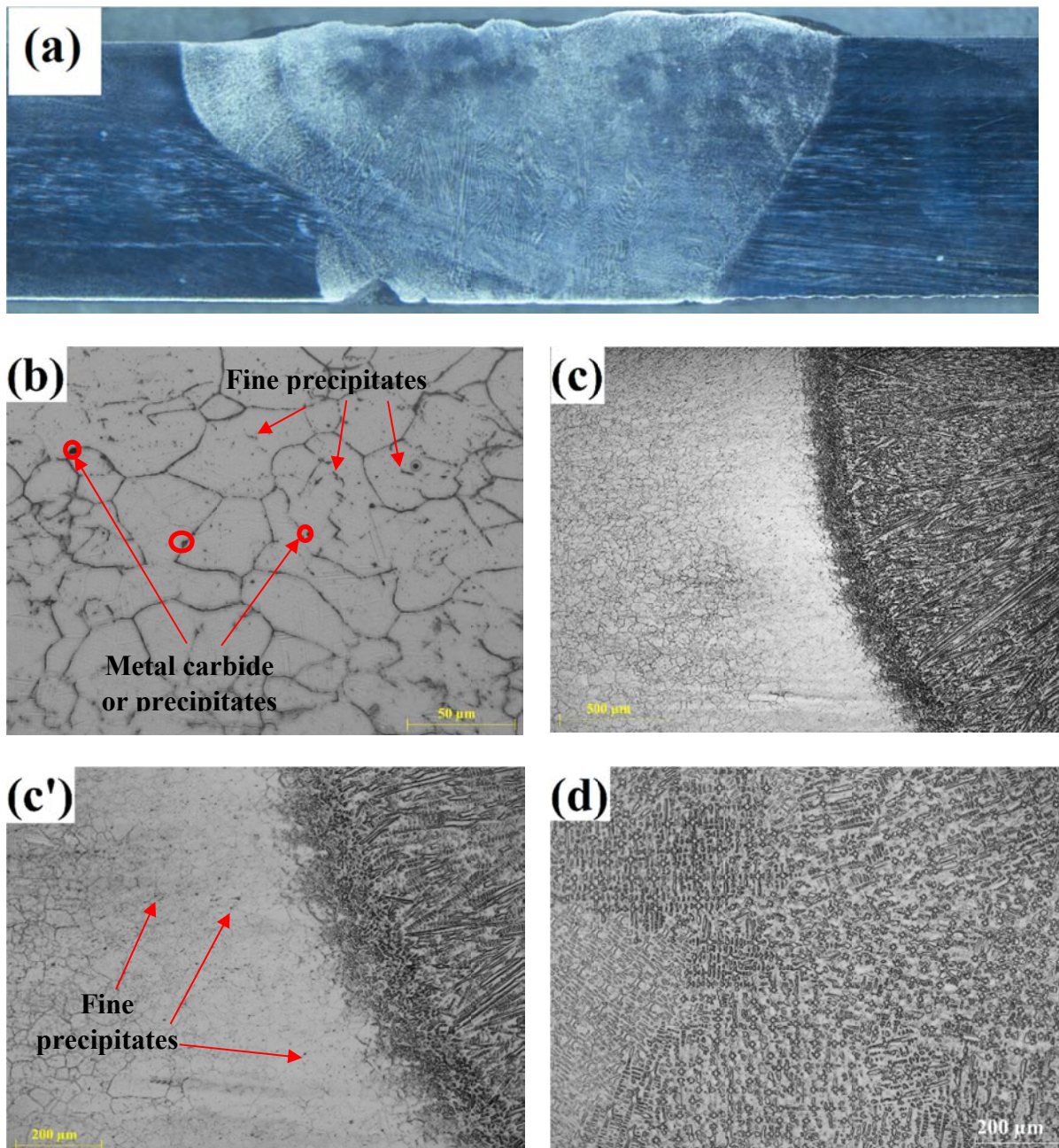
### 3. Results and discussion

#### 3.1. Microstructure evaluation

Fig. 2a shows the weld cross section view of the IAPAWed Inconel 625 plate. Fig. 2b shows the BM microstructure, comprising coarse equiaxed grain structure. Some precipitates were observed in the BM austenitic matrix (Fig. 2b). These precipitates were categorised as metal carbides and metal rich secondary

phases like Cr-rich, Mo-rich, and Nb-rich. Fig. 2(c-c') displays the HAZ near the fusion boundary, where the grains are not clearly revealed. The HAZ may experience a higher temperature range during the welding, due to which the grains of the BM may dissolve. Detailed analysis indicated an approximately 470  $\mu\text{m}$  wide white band of the HAZ near the fusion boundary, as shown in Fig. 2c. However, carbides were still found in the HAZ region (as shown in Fig. 2c') because of their relatively higher dissolution temperature.

Fig. 2c' shows the transition zone of the fusion boundary, which contains columnar dendritic structures directed perpendicular to the fusion boundary. Three different types of dendritic structure were present in the FZ, i.e., firstly a higher amount of continuous columnar dendritic structure (Fig. 2f), secondly equiaxed dendritic structure (Fig. 2g), and thirdly low amount of fine dendritic structure (Fig. 2h). The heat input variation had



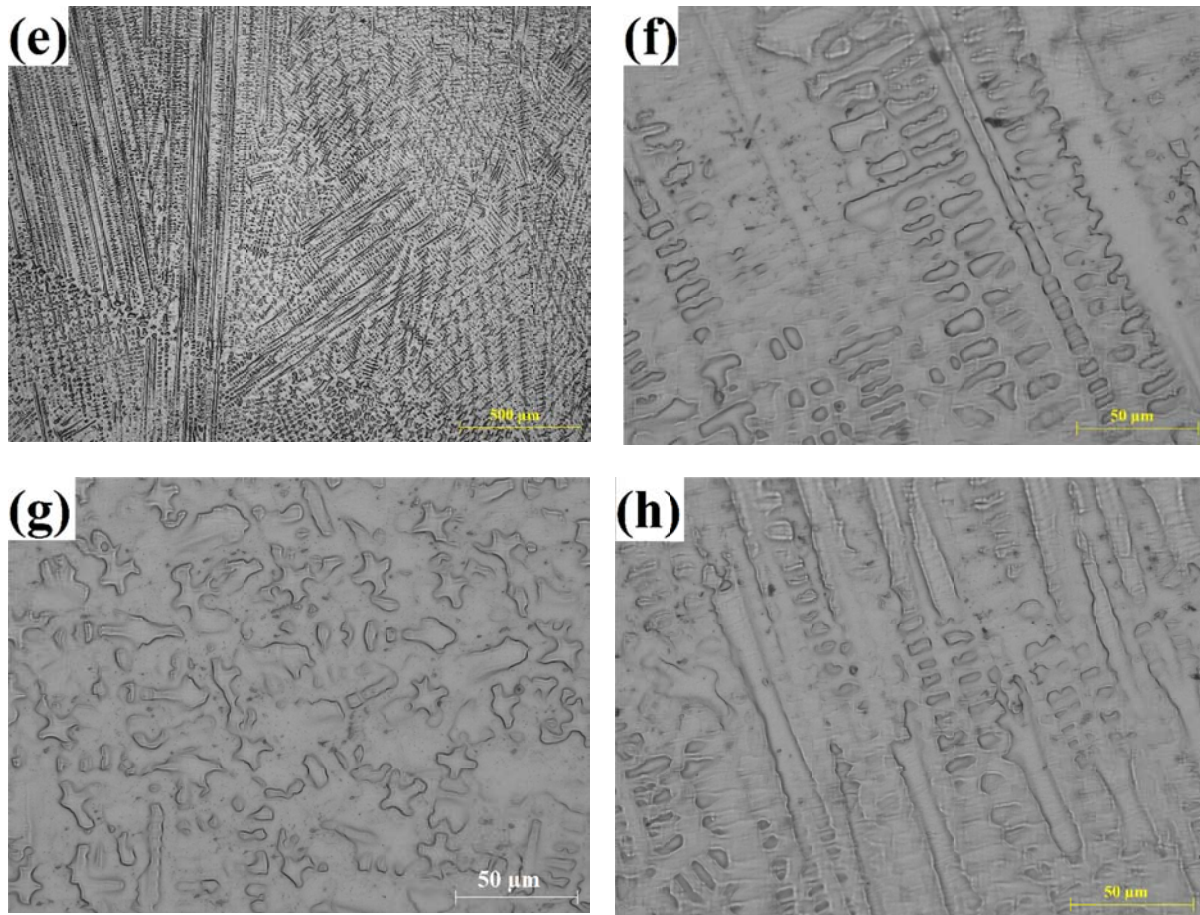


Fig. 2. Microstructure of IAPAW welded Inconel 625 alloy (a) macro view of weld cross-section, (b) BM at 50 $\times$ , (c) HAZ at 10 $\times$ , (c') transition zone of HAZ and FZ at 50 $\times$ , (d) first zone of FZ at 10 $\times$  (e) second zone of FZ at 10 $\times$ , three different dendritic structure zones of FZ shows at 50 $\times$  shown in (f), (g), and (h)

an essential role in the formation of different microstructures in the FZ [22]. The middle of the FZ contained equiaxed dendrite structure and fine columnar dendritic structure, which is squeezed between the long columnar dendrite along the weld direction.

The Fig. 3(a-e) and TABLE 3 show the EDX point analysis of various welded zones. In Fig. 3(a', b' and c') shows the magnified view of different dendrites and the Laves phase in the FZ. The point analysis showed less Nb present in the dendritic core (composition of points 1, 4 and 7 are mentioned in TABLE 3). The Nb was rejected due to reduced solid solubility of Nb in  $\gamma$ -Ni matrix. This leads to the formation of Nb-rich brittle

phase in the interdendritic region [23]. This micro segregation of elements found in the FZ is due to high heat input and slow solidification rate of the molten pool [24], and thereby developed a high amount of Laves phase, as shown in points 2,3,5,6 and 8, composition are mentioned in TABLE 3. The brittle and hard Laves phase always appears in the interdendritic area in fusion welding [23-24]. It deteriorates the properties and plasticity of the FZ. Richards et al. [11] indicated the Laves phase chemical composition as  $A_2B$  (A: Ni/Fe/Cr, B: Nb/Mo/Ti), type. A higher amount of Laves phase is prone to crack initiation and propagation during tensile loading [23,24,26,27]. The composition of the

EDX analysis of the FZ of IAPAWed Inconel 625

TABLE 3

Element	Wt. (%)										
	P1	P2	P3	P4	P5	P6	P7	P8	P9	A1	A2
Nb	1.7	20.0	69.1	1.7	16.4	57.4	1.6	19.3	3.3	3.9	3.81
Mo	7.2	18.7	6.7	8.3	17.7	8.7	7.1	19.5	8.2	8.9	8.85
Cr	20.1	16.9	6.9	20.8	17.0	9.9	23.3	17.1	23.1	21.9	24.29
Mn	—	0.2	0.6	0.4	0.6	0.4	—	0.1	—	—	0.70
Fe	5.2	2.6	0.2	4.6	3.5	1.0	4.6	2.5	5.1	3.9	5.00
Ni	65.2	41.4	10.8	63.7	44.6	19.3	63.0	41.1	59.7	61.0	56.60
Ti	0.5	0.2	5.3	0.2	0.1	2.6	—	—	0.3	—	0.44
Al	0.2	—	0.4	0.2	0.2	0.7	0.3	0.3	0.2	0.3	0.31

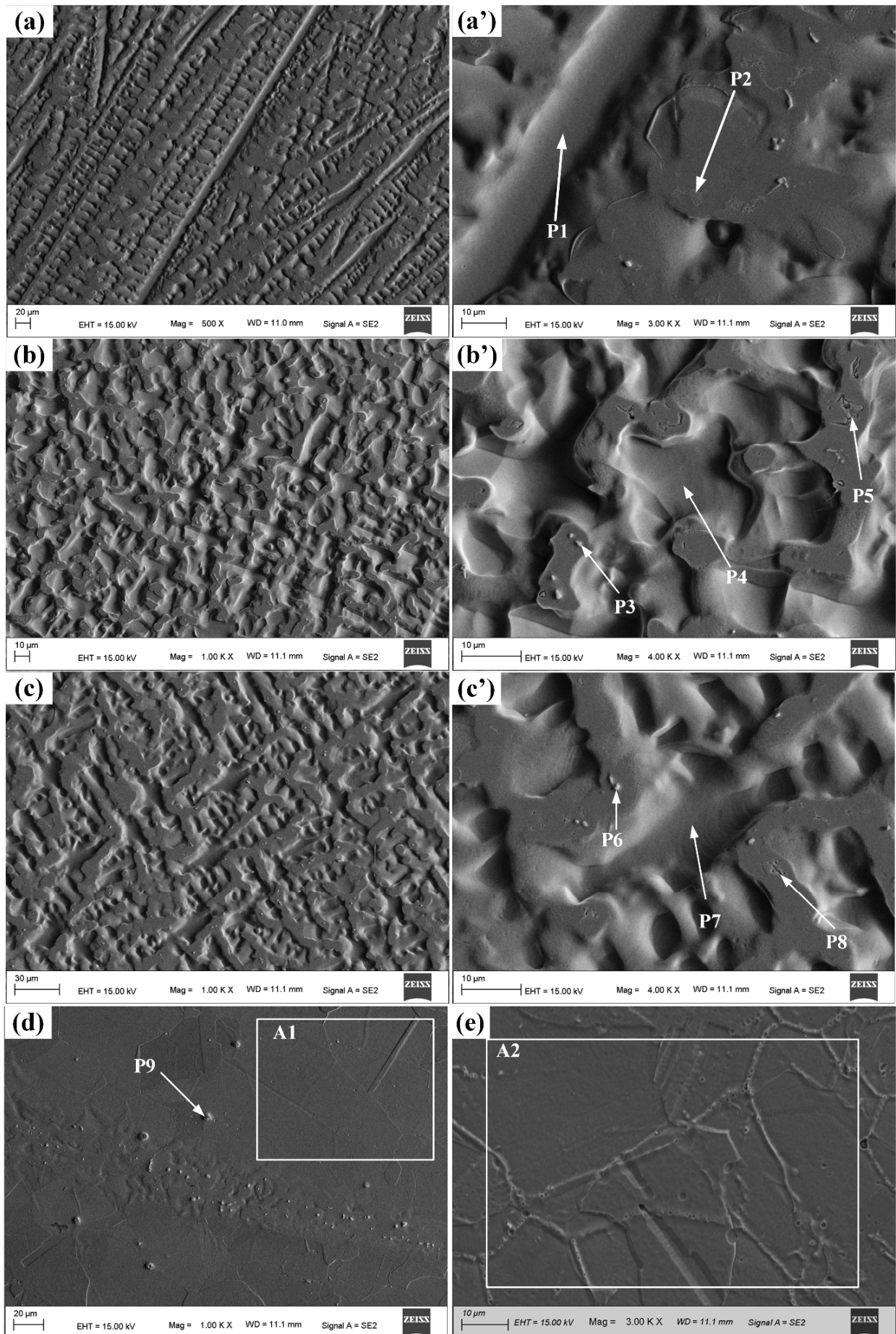


Fig. 3. EDX analysis of the various zones of the IAPAW welded sample (a) FZ 1, (b) FZ 2, (c) FZ 3, (d) HAZ and (e) BM

HAZ and the BM are almost similar, reported in Fig. 3(d and e) and TABLE 3. Tensile properties of the weld are significantly influence by Laves phase.

### 3.2. X-ray diffraction

To study the influence of IAPAW on the features of phase structure, the XRD analysis was carried out. Fig. 4a shows the XRD spectra of various zones of the Inconel 625 welded specimen. The XRD plot revealed dominant mixture of a typical Ni–Cr–Mo austenite ( $\gamma$ ) phase throughout the welded zone [28]. It indicated that all the zones have almost same crystal structure. Inconel 625 is a solid solution strengthening superalloy; phase transition or formation of metal carbide is usually occurred during fusion welding [29]. The volume fraction of carbide formation may be less than identifying threshold by the XRD analysis [29]. In higher temperatures, some intermetallic phases like  $\delta$  ( $\text{Ni}_3\text{Nb}$ ),  $\gamma'$  ( $\text{Ni}_3\text{Al}$ ,  $\text{Ni}_3\text{Ti}$ ),  $\gamma''$  ( $\text{Ni}_3\text{Nb}$ ), Laves phase, and metallic carbide are precipitated in the Ni base austenitic matrix. But among them, the formation of  $\delta$ ,  $\gamma'$ , and  $\gamma''$  phases are not possible in the FZ due to rapid solidification. However, the presence of all phases are feasible in the BM, because it passes through the several heat treatment and mechanical rolling process. So, detection of these phases are challenging by XRD scan because these precipitates have similar crystalline nature and overlap with the Ni–Cr–Mo phase and austenite ( $\gamma$ ) matrix [29]. A detailed investigation was carried out on the XRD scan data related to peak broadening and shifting.

The lattice parameter of the various zones were calculated and mentioned in TABLE 4. It is found that the lattice parameter

value is highest at the BM and lowest at the HAZ. The presence of metal carbide and other precipitate phases in the BM zone (as shown in Fig. 3e) produced high lattice parameter. The formation of carbides and high Laves phase reduced the lattice parameter size of the FZ. The lattice constant size of the HAZ is lower than the other zones of welded material. The recrystallization, minor formation of Laves phase and dissolution of some parent material precipitates (as shown in Fig. 3d) caused lowering in the lattice parameter.

Fig. 4b represents the peak shifting of the diffraction patterns of the BM, HAZ, and FZ. Peaks shifted towards higher angles and peak sharp with reduces broadening of the FZ specimen. The high intensity and broadening of the peak of the FZ is due to the rearrangement of the crystal structure. The peaks shifting might be related to the development of thermal stress (compressive) and/or micro-segregation and/or precipitate formation in the microstructure (causing depletion of Nb and Mo elements from Ni ( $\gamma$ ) matrix) [30].

### 3.3. Tensile test analysis

Fig. 5 shows the tensile failure of the welded specimen, where the fracture is located at the middle of the FZ. TABLE 5 provides information on ultimate tensile strength, yield strength, and % elongation of the welded specimen. The yield stress and ultimate tensile stress of the welded specimen were 412 MPa and 658 MPa, respectively. The joint efficiency is much less than other published literature [2]. This is because of higher amount of Laves phase presence in the FZ and the higher area of the FZ. The EDX analysis exhibited formation of interdendritic Laves

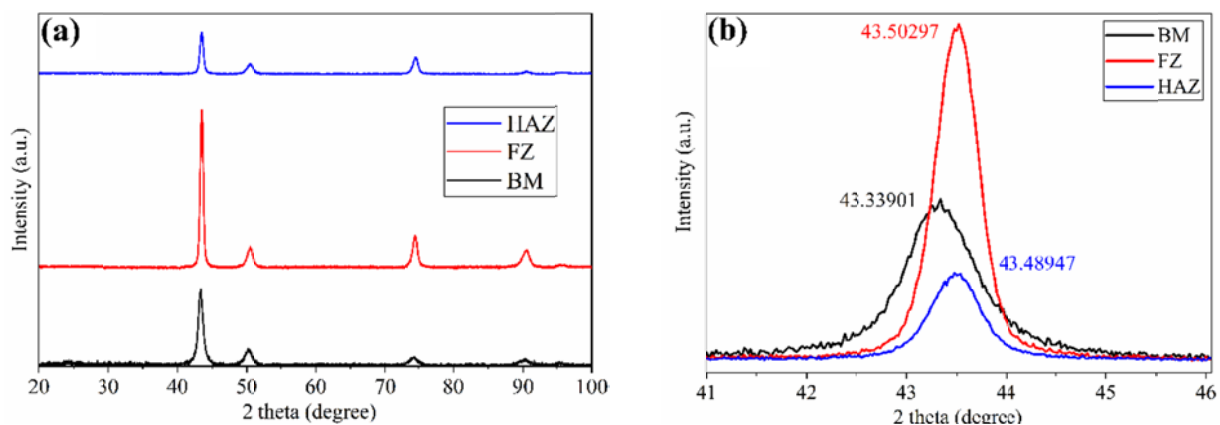


Fig. 4. XRD analysis of the various zones of the IAPAW welded sample

TABLE 4

Calculated average Lattice parameter, micro strain, and crystalline size of the weldment obtained from Diffraction results

Different Zones	Peak position for crystallography planes of the matrix (1 1 1)	Lattice parameter ( $\text{\AA}$ )	Micro-strain ( $\mu\epsilon$ )	Crystallite size ( $\text{\AA}$ )
FZ	43.50297	3.601529863	4.71	926.08
HAZ	43.48947	3.600040176	2.67	219.65
BM	43.33901	3.610735493	4.89	168.59

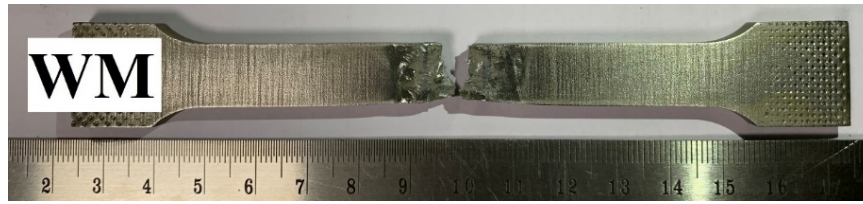


Fig. 5. Tensile failed specimen of the welded joint

phase in the FZ (as shown in Fig. 3(a'-c')), which significantly reduced the elongation of the weldments compared to the BM. This leads to failure at the middle of the FZ during tensile test, as represented in Fig. 5.

TABLE 5

The BM and welded specimen's mechanical properties

Material	Yield stress, $\sigma_{YS}$ (MPa)	Ultimate tensile stress, $\sigma_{UTS}$ (MPa)	% Elongation
Welded	412	658	10

Fig. 6(a-b) shows a FESEM picture of the tensile fracture surface. In Fig. 6a, the size of the dimple is large, which attributes brittle failure mode. Figure 6b shows an enlarged view of the brittle failure region. The fracture surface is entirely free of micro voids or pores, indicating absents of micro-cracks or inclusions.

#### 4. Conclusion

The IAPAW process was useful to weld thick Inconel 625 metal plate. The welding was achieved by 135 A of welding current and a preheat arrangement by high-frequency induction heat setup. The following conclusions can be made from the present invitation.

1. Microstructure studies of the FZ showed variety of dendritic structures. The FESEM and EDX analysis showed a higher percentage of Laves phase in the FZ. The Laves

phase contained high amount of Nb. In the dendritic core, the Nb concentration is less than the BM matrix. A bright width zone was observed in the HAZ with metal carbides and other precipitates in the austenitic matrix.

2. The diffraction peak of the (111) plane showed the peak shifting that occurred in the FZ due to developed thermal stress and the depletion of Nb and Mo concentration in the Ni-matrix. Higher micro strain was observed in the FZ.
3. The weld joint UTS was 658 MPa and 10% elongation. The welded tensile specimen was failed in the FZ due to the presence of high amount of Laves phase. The tensile fracture surface of the FZ showed brittle mode of failure.

#### REFERENCE

- [1] R.I. Badiger, S. Narendranath, M.S. Srinath, Joining of Inconel-625 alloy through microwave hybrid heating and its characterization. *J. Manuf. Process.* **18**, 117-123 (2015).
- [2] K.D. Ramkumar, S.S. Mulimani, K. Ankit, A. Kothari, S. Ganguly, Effect of grain boundary precipitation on the mechanical integrity of EBW joints of Inconel 625. *Mater. Sci. Eng. A.* **808**, 140926 (2021).
- [3] J.N. DuPont, C.V. Robino, J.R. Michael, M.R. Nous, A.R. Marder, Solidification of Nb-bearing superalloys: Part I. Reaction sequences. *Metall. Mater. Trans. A.* **29** (11), 2785-2796 (1998).
- [4] A.N. Ebrahimi, N.B.M. Arab, M.H. Gollo, Thermal analysis of laser beam welding of nickel-based super alloy Inconel 625 to AISI 316L, using Gaussian optics theory in keyhole. *J. Brazilian Soc. Mech. Sci. Eng.* **38** (4), 1199-1206 (2016).

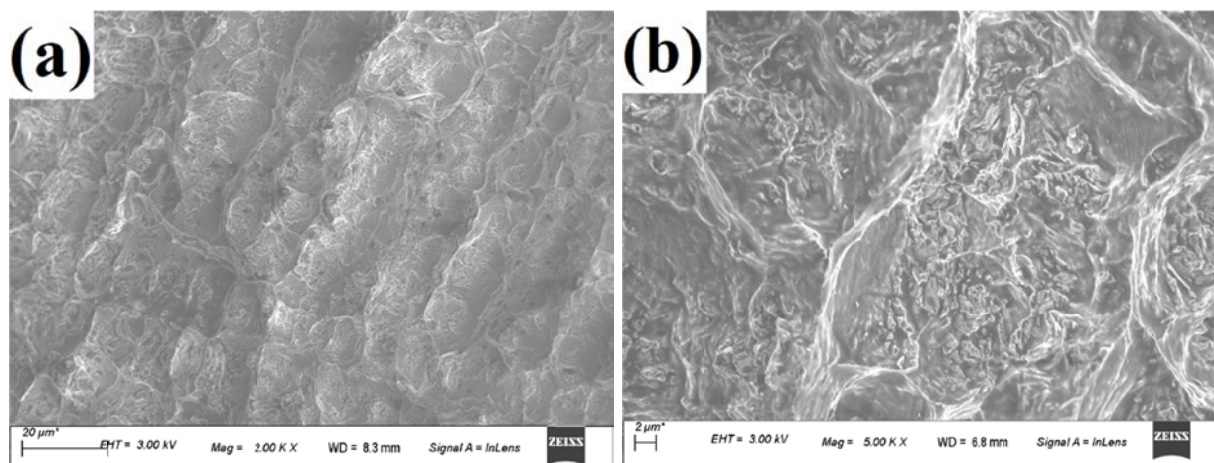


Fig. 6. FESEM images of a tensile fracture surface of the welded specimen at (a) 2000 KX and (b) 5000 KX

- [5] J. Sivakumar, N.N. Korra, Optimization of Welding Process Parameters for Activated Tungsten Inert Welding of Inconel 625 Using the Technique for Order Preference by Similarity to Ideal Solution Methodology. *Arab. J. Sci. Eng.* **46** (8), 7399-7409 (2021).
- [6] K.H. Song, W.Y. Kim, K. Nakata, Evaluation of microstructures and mechanical properties of friction stir welded lap joints of Inconel 600/SS 400. *Mater. Des.* **35**, 126-132 (2012).
- [7] M.F. Chiang, C. Chen, Induction-assisted laser welding of IN-738 nickel-base superalloy. *Mater. Chem. Phys.* **114** (1), 415-419 (2009).
- [8] A. Ikram, N. Arif, H. Chung, Design of an induction system for induction assisted alternating current gas metal arc welding. *J. Mater. Process.* **231**, 162-170 (2016).
- [9] H.R. Zareie Rajani, S.A.A. Akbari Mousavi, The effect of explosive welding parameters on metallurgical and mechanical interfacial features of Inconel 625/plain carbon steel bimetal plate. *Mater. Sci. Eng. A.* **556**, 454-464 (2012).
- [10] J.W. Han, S.H. Jung, H. Cho, H.W. Lee, Investigation of the weld properties of Inconel 625 based on Nb Content. *Int. J. Electrochem. Sci.* **13**, 2829-2841 (2018).
- [11] N.L. Richards, X. Huang, M.C. Chaturvedi, Heat affected zone cracking in cast inconel 718. *Mater. Character.* **28** (4), 179-187 (1992).
- [12] J. Sivakumar, N.N. Korra, P. Vasantharaja, Computation of residual stresses, distortion, and thermogravimetric analysis of Inconel 625 weld joints. *Proc. Inst. Mech. Eng. Part C J. Mech. Eng. Sci.* **235** (19), 4109-4118 (2021).
- [13] N. Arif, H. Chung, Alternating current-gas metal arc welding for application to thick plates. *J. Mater. Process. Technol.* **222**, 75-83 (2015).
- [14] R.S. Coelho, M. Corpas, J.A. Moreto, A. Jahn, J. Standfuß, A. Kaysser-Pyzalla, H. Pinto, Induction-assisted laser beam welding of a thermomechanically rolled HSLA S500MC steel: A microstructure and residual stress assessment. *Mater. Sci. Eng. A.* **578**, 125-133 (2013).
- [15] R. Sun, Y. Shi, Y. Yang, X. Wang, X. Zhou, Microstructure, element segregation and performance of Inconel 625 metal layer deposited by laser-assisted ultra-high frequency induction deposition. *Surf. Coat. Technol.* **405**, 126715 (2021).
- [16] R.K.B. Meitei, P. Maji, A. Samadhiya, R. Karmakar, S.K. Ghosh, S.C. Saha, An experimental investigation on joining of copper and stainless steel by induction welding technique. *Int. J. Precis. Eng. Manuf.* **21**, 613-621 (2020).
- [17] B.M. R.K., P. Maji, A. Samadhiya, S.K. Ghosh, B.S. Roy, A.K. Das, S.C. Saha, A study on induction welding of mild steel and copper with flux under applied load condition. *J. Manuf. Process.* **34**, 435-441 (2018).
- [18] T. Bayerl, M. Duhovic, P. Mitschang, D. Bhattacharyya, The heating of polymer composites by electromagnetic induction – a review. *Compos Part A Appl Sci Manuf.* **57**, 27-40 (2014).
- [19] N. Sommer, S. Böhm, Laser-induction welding of nodular grey cast iron using oscillating beam guidance-microstructural and mechanical characterization. *J. Advanced Joining Process.* **5**, 100078 (2022).
- [20] S. Raj, P. Biswas, High-frequency induction assisted hybrid friction stir welding of Inconel 718 plates. *J. Manuf. Sci. Eng.* **144**, 1-15 (2021).
- [21] H.T. Zhang, X.Y. Dai, J.C. Feng, L.L. Hu, Preliminary investigation on real-time induction heating-assisted underwater wet welding. *J. Weld.* **1**, 8-15 (2015).
- [22] S. Kou, *Welding Metallurgy*, 2nd Edition, 2003.
- [23] S.G.K. Manikandan, D. Sivakumar, K. Prasad Rao, M. Kamaraj, Laves phase in alloy 718 fusion zone - Microscopic and calorimetric studies. *Mater. Character.* **100**, 192-206 (2015).
- [24] S.K. Rai, A. Kumar, V. Shankar, T. Jayakumar, K.B.S. Rao, B. Raj, Characterization of microstructures in Inconel 625 using X-ray diffraction peak broadening and lattice parameter measurements. *Scr. Mater.* **51**, 59-63 (2004).
- [25] G. Li, J. Huang, Y. Wu, An investigation on microstructure and properties of dissimilar welded Inconel 625 and SUS 304 using high-power CO<sub>2</sub> laser. *Int. J. Adv. Manuf. Technol.* **76** (5-8), 1203-1214 (2015).
- [26] C. Radhakrishna, K. Prasad Rao, The formation and control of Laves phase in superalloy 718 welds. *J. Mater. Sci.* **32** (8), 1977-1984 (1997).
- [27] S. Dev, K.D. Ramkumar, N. Arivazhagan, R. Rajendran, Investigations on the microstructure and mechanical properties of dissimilar welds of inconel 718 and sulphur rich martensitic stainless steel, AISI 416. *J. Manuf. Process.* **32**, 685-698 (2018).
- [28] K. Sivaprasad, S. Ganesh Sundara Raman, Influence of weld cooling rate on microstructure and mechanical properties of alloy 718 weldments. *Metall. Mater. Trans. A.* **39** (9), 2115-2127 (2008).
- [29] M. Sharifitabar, S. Khorshahian, M.S. Afarani, P. Kumar, N.K. Jain, High-temperature oxidation performance of Inconel 625 superalloy fabricated by wire arc additive manufacturing. *Corros. Sci.* **197**, 110087 (2022).
- [30] R. Jiang, A. Mostafaei, J. Pauza, C. Kantzos, A.D. Rollett, Varied heat treatments and properties of laser powder bed printed Inconel 718. *Mater. Sci. Eng. A.* **755**, 170-180 (2019).